

Article

Investigation of the Energy-Saving Potential of Buildings with Radiative Roofs and Low-E Windows in China

Lin-Rui Jia ^{1,2} , Qing-Yun Li ³, Jie Yang ⁴, Jie Han ^{1,*}, Chi-Chung Lee ^{1,*}  and Jian-Heng Chen ⁵

¹ School of Science and Technology, Hong Kong Metropolitan University, Hong Kong, China; 17865163055@163.com

² Department of Building Environment and Energy Engineering, The Hong Kong Polytechnic University, Hong Kong, China

³ Teaching and Learning Centre, Lingnan University, Hong Kong, China

⁴ Joinhuger Group Co. Ltd., Weifang 261000, China

⁵ School of Energy and Environment, City University of Hong Kong, Hong Kong, China

* Correspondence: chan@hkmu.edu.hk (J.H.); clee@hkmu.edu.hk (C.-C.L.)

Abstract: This study develops a model for buildings with a cooling roof, walls, and low-emissivity (Low-E) windows. This model is verified through experimental analysis. The cooling demands of standard buildings and cooling buildings are compared, and the energy-saving potentials of cooling buildings are analysed. It is found that compared to standard buildings, cooling buildings exhibit superior cooling performances attributable to the application of cooling materials. Considering Hong Kong's weather data, the indoor temperature of cooling buildings can be sub-ambient. The cooling demands of cooling buildings are decreased from 75 W/m² to 30 W/m², indicating a 60% energy-saving potential. The nationwide cooling demand for a standard building across China is approximately 95.7 W/m², whereas the nationwide summer average cooling demand for cooling buildings is 52.7 W/m². Moreover, the cooling performance of a cooling roof is adversely affected by hot and humid weather conditions, resulting in lower temperature drops in southern regions compared to northern regions. However, the nationwide temperature drop across China can still be 1.6 °C, demonstrating promising cooling potentials. For the Low-E windows, the temperature can also be sub-ambient, with a nationwide average temperature drop of 1.7 °C. Therefore, the use of Low-E windows across China can also significantly contribute to energy savings for indoor cooling. Overall, the results of this study show that cooling buildings have high energy-saving potential under various climates. The proposed model can provide a reliable tool to facilitate relevant cooling evaluation by stakeholders, thereby benefiting the popularization of this technology.

Keywords: sky cooling; cooling coating; Low-E window; energy saving; cooling map



Citation: Jia, L.-R.; Li, Q.-Y.; Yang, J.; Han, J.; Lee, C.-C.; Chen, J.-H. Investigation of the Energy-Saving Potential of Buildings with Radiative Roofs and Low-E Windows in China. *Sustainability* **2024**, *16*, 148. <https://doi.org/10.3390/su16010148>

Academic Editor: Chi-Ming Lai

Received: 11 November 2023

Revised: 16 December 2023

Accepted: 21 December 2023

Published: 22 December 2023



Copyright: © 2023 by the authors. Licensee MDPI, Basel, Switzerland. This article is an open access article distributed under the terms and conditions of the Creative Commons Attribution (CC BY) license (<https://creativecommons.org/licenses/by/4.0/>).

1. Introduction

The world is currently facing an energy crisis due to the increasing global demand for energy, limited fossil fuel resources, and concerns over climate change. This crisis manifests as escalating energy costs, energy deficits, and an urgent need for alternative energy sources. In addition to developing alternative energy sources, it is important to focus on energy conservation and efficiency. One promising technology in this area is passive sky cooling, which has the potential to decrease the energy required for cooling buildings and other infrastructures.

In 1970, passive radiative sky cooling (RSC) with no energy input was introduced as a reasonable method for dealing with the energy crisis [1,2]. RSC is a radiative heat transfer, which mainly relies on the far-infrared thermal radiation in the atmospheric window (8–13 μm) [1,2]. This sort of heat transfer process happens spontaneously for any objects with a surface temperature greater than 0 Kelvin through the emission of electromagnetic

waves. The average earth temperature (288 Kelvin) significantly exceeds the deep space temperature of 3 Kelvin [3].

Previous studies mainly focused on night-time sky-cooling technologies due to the drawbacks of materials with smaller solar reflectance [4,5]. With rapid advances in metamaterials [6], microsphere-based material designs [7] and nanophotonics [8], daytime radiative cooling materials have been developed. Newly fabricated cooling coatings exhibit high reflectance for solar radiation within the range of 0.3–2.5 μm . For example, Raman et al. [8] used a thermal–photonic approach and then fabricated a seven-layered cooler (comprising SiO_2 and HfO_2). This novel coating feature with a solar reflectance of 0.97 is capable of achieving a net cooling power of 40.1 W/m^2 and a temperature drop of 4.9 $^\circ\text{C}$ below ambient temperature. In addition, similar studies have focused on developing cooling coatings with comparable spectral properties with a solar reflectance of over at least 0.96 and a far-infrared thermal emittance greater than 0.78 [6,9,10]. In actual applications, these cooling coatings are typically used passively by directly applying them to objects requiring cooling, such as roofs [11–13] and solar cell applications [2,14].

Low-emissivity (Low-E) windows have gained significant attention in the field of energy-efficient building design [15]. These windows are designed to minimize heat transfer through the glass, thereby enhancing thermal insulation and reducing energy consumption [16]. Significant advancements have been made in the development of Low-E windows in recent years, leading to improved performance and a broader range of options for building designers and homeowners. Noteworthy technological progressions include double and triple glazing [17], spectrally selective coatings [18], and ventilated windows [19]. Low-E windows offer numerous benefits in terms of energy efficiency, occupant comfort, and environmental sustainability, such as improved thermal insulation, energy savings, enhanced indoor comfort, and ultraviolet (UV) protection [20].

Currently, some studies have investigated the energy-saving potential of integrating these passive cooling technologies in building fields. For instance, Zhu et al. [21] investigated the cooling power potentials of cooling roofs at ambient temperature levels across China. Several innovative cool roof systems have been suggested to enhance building cooling. For example, Yew et al. [12] introduced a novel cool roof system that incorporates a dynamic air cavity, effectively enhancing the cooling capacity of the attic air temperature. The implementation of cool roofs offers numerous advantages, such as decreased cooling energy consumption, reduced carbon emissions, mitigated air pollution, and the alleviation of urban heat island issues through passive thermal management techniques. Similar studies have been carried out in Britain, Greece, Singapore, France, Italy, Japan, Malaysia, and so forth [22]. Few studies have been performed in China, which limits the popularization in China, which has huge cooling demands. For Low-E windows, current studies [23,24] have focused on the heat transfer of the window itself. The influence of the thermal capacity of the indoor environment on the window's performance and the overall relationships among cooling roofs, walls, and windows are not clear.

In addition, current studies investigating the energy-saving potentials for using these cooling technologies separately in buildings have failed to explore the integral cooling performances. Moreover, the performance of cooling roofs and Low-E windows is significantly affected by the weather conditions. However, limited research has focused on their cooling performances under varied climatic conditions. Therefore, the performances of cooling roofs and Low-E windows across China should be better assessed.

Thus, this study develops a model for buildings with cooling roofs, walls, and Low-E windows. The developed model is verified with experimental data. The cooling demands of standard buildings and cooling buildings are compared, and the energy-saving potential of cooling buildings is analysed. Detailed elaboration is provided on the cooling performances of cooling roofs and Low-E windows. The importance of cooling buildings cannot be overstated, given their direct influence on occupant comfort, health, and productivity and the lifespan of equipment and infrastructure. Furthermore, as the world grapples

with the challenges of climate change and escalating energy demands, this study offers an energy-efficient solution for indoor cooling.

2. Model Description

Figure 1 shows the schematic diagram of the building model. The model comprises four parts, including the building roof, walls, and windows. On the external surfaces of the roof and walls, a cooling coating is painted on to reduce solar absorption and increase the outgoing radiative power to reduce indoor cooling demands. In addition, low-energy (Low-E) windows are used in the building because most of the heat absorbed by the indoor environment is through the windows. Thus, using Low-E windows that allow visible light into the indoor area but limit the infrared thermal radiation from the environment is necessary. Low-E windows include two layers of glass, which are the indoor-side glass and outdoor-side glass. The cooling coating polymer is painted on the outdoor-side glass, which has been proven to reduce the indoor temperature. The diagram is shown in Figure 1. Tables 1 and 2 list the settings and thermal properties of the building, respectively.

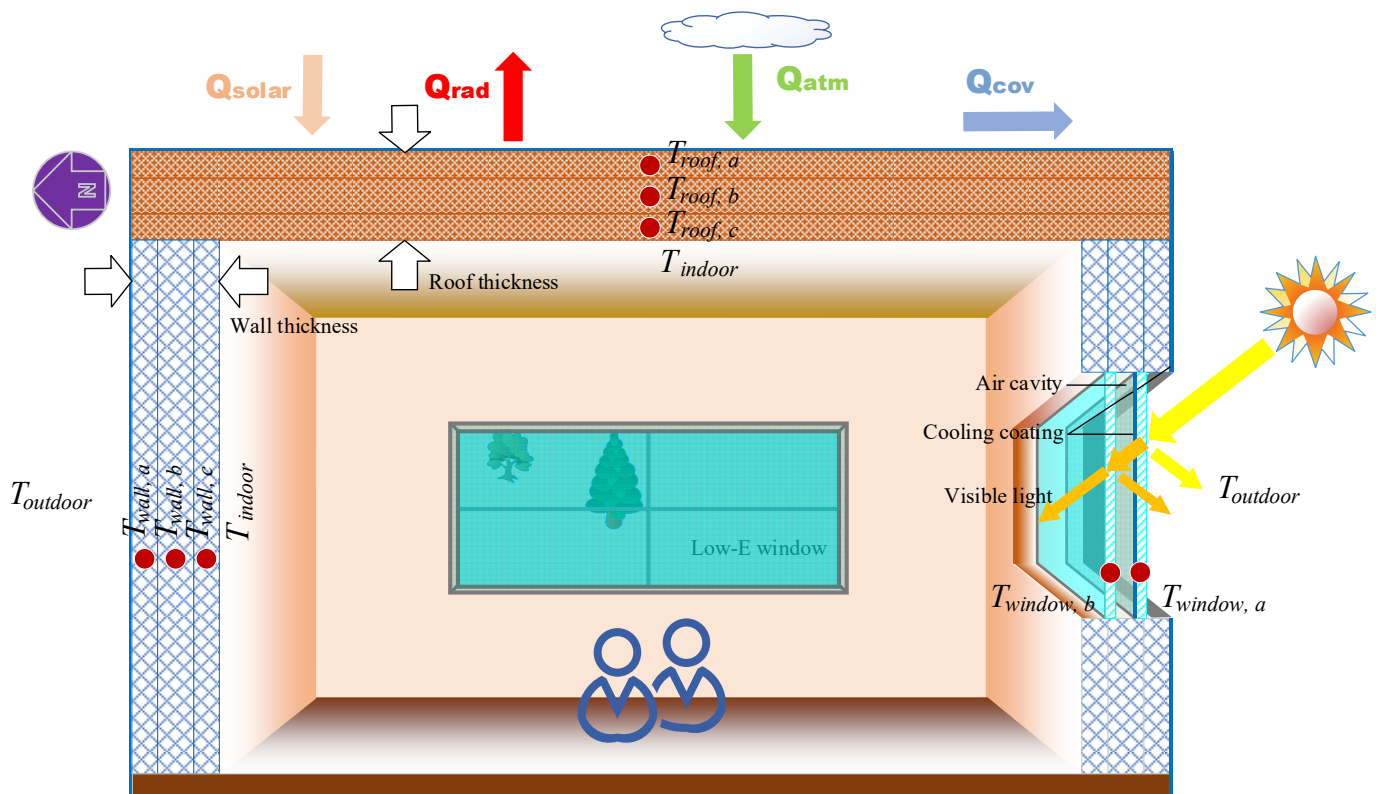


Figure 1. Schematic diagram of the building model.

Table 1. Settings of the building model.

Item	Description
Floor area	100 m ²
Window-to-wall ratio	0.5
Number of floors	1
Roof structure	Roof membrane + Roof insulation + Metal decking
Wall structure	Stucco + Gypsum board + Wall insulation + Gypsum board

Table 2. Thermal properties of the building model [25].

Structure	Material Name	Thickness m	Conductivity (W/m/K)	Density (kg/m ³)	Specific Heat (J/kg/K)
Roof	F13 built-up roofing	0.0095	0.16	1120	1460
	Roof insulation	/	4.3	/	/
	F08 metal	0.0008	45.28	7824	500
Wall	F07 stucco	0.0254	0.72	1856	840
	G01 gypsum board	0.0159	0.16	800	1090
	Wall insulation	/	1.9	/	/
	G01 gypsum board	0.0159	0.16	800	1090
Windows	/	0.006	1.0	2600	720

3. Model Development

In this study, the finite difference method is used to develop the models, including the roof model and the four-direction wall and window models. The finite difference method is based on the thermal balance theory that the internal energy equals the difference between the absorbed delimited energy. This method shows high calculation accuracy and calculation efficiency and, thus, is used in this study.

3.1. Roof Model

The numerical method is used to develop the building model. Overall, there are four parts in the model, namely, the roof model, wall model, window model, and floor model.

Due to the larger cooling capacity of the building roof, the roof model is established first. On the outdoor side roof, the roof exchanges heat with the inner roof (ceiling) and the ambient environment. Thus, the control equation of the outdoor-side roof heat transfer can be expressed by:

$$\rho_{roof}c_{roof}V_{roof}\frac{dT_{roof}}{dt} = k_{roof}\frac{dT_{roof}}{dy}dx + A_{roof}Q_{net,roof} \quad (1)$$

where ρ_{roof} , c_{roof} , and V_{roof} are the density, specific heat capacity, and volume, respectively. The corresponding units are kg/m³, J/kg/K, and m³, respectively. k_{roof} is the thermal conductivity of the roof, W/m/K. T_{roof} is the roof temperature, °C. t is the operation time, s. A_{roof} is the roof area, m². $Q_{net,roof}$ is the net cooling power of the building roof, W/m², which is introduced in Equation (4).

Thermal conduction exists between the top roof layer and the ceiling, and the control equation can be expressed as:

$$\rho_{roof}c_{roof}V_{roof}\frac{dT_{roof}}{dt} = k_{roof}\frac{dT_{roof}}{dy}dx \quad (2)$$

where y is the vertical coordinate, m, and x is the horizontal coordinate, m.

The ceiling exchanges heat with the indoor environment. The indoor-side roof temperature can be calculated by:

$$\rho_{roof}c_{roof}V_{roof}\frac{dT_{roof}}{dt} = k_{roof}\frac{dT_{roof}}{dy}dx + A_{roof}Q_{ceiling} \quad (3)$$

where A_{roof} is the ceiling area, m². $Q_{ceiling}$ is the heat exchange rate at the ceiling, W/m², which can be calculated with Equation (17).

The $Q_{net,roof}$ is the net cooling power on the building roof, W/m². On the building roof, the roof exchanges heat with the environment by radiative and convective heat transfer. The radiative heat transfer incorporates short-wave incoming solar radiation (Q_{solar}), long-wave radiated-out radiative heat (Q_{rad}), and downwelling atmospheric heat (Q_{atm}). In addition, the top roof also exchanges convective heat with the ambient environment ($Q_{convection}$).

According to energy balance theory, the net cooling power $Q_{net,roof}$ equals the radiated-out cooling power minus the absorbed cooling power, which thus can be calculated by:

$$\begin{cases} Q_{net,roof} = Q_{radiation} - Q_{convection} \\ Q_{radiation} = Q_{rad} - Q_{atm} - Q_{solar} \end{cases} \quad (4)$$

The Q_{rad} means the long-wave radiated-out radiative heat on the top roof surface, which can be calculated by:

$$Q_{rad} = 2\pi \int_0^{0.5\pi} \sin\theta \cos\theta d\theta \int_0^\infty I_{BB}\left(\left(T_{roof} + 273.15\right), \lambda\right) \varepsilon_{cc}(\lambda, \theta) d\lambda \quad (5)$$

where ε_{cc} is emittance of the top roof surface. θ is the zenith angle, °. λ is the wavelength, m.

The radiative cooling power Q_{rad} is a function of $(T_{roof} + 273.15)$. $I_{BB}(T_{roof} + 273.15, \lambda)$ is the standard thermal radiance of the blackbody, $W/(sr \cdot m^3)$.

$$I_{BB}\left(\left(T_{roof} + 273.15\right), \lambda\right) = \frac{2\bar{h}v_1^2}{\lambda^5} \frac{1}{\exp\left(\frac{\bar{h}v_1}{\lambda\varphi(T_{roof} + 273.15)}\right) - 1} \quad (6)$$

where \bar{h} and φ are the Planck constant and Boltzmann constant, J·s and J/K, respectively; v_1 is the light velocity in vacuum space, m/s; and λ is the spectral wavelength, m.

In order to calculate the downwelling atmospheric longwave radiation received at the earth's surface, clear-sky and cloudy-sky conditions must be considered. Thus, the downwelling atmospheric radiation absorbed by the top surface of the roof can be calculated by:

$$Q_{atm} = (1 - \xi)Q_{atm,clear} + \xi \cdot Q_{atm,cloudy} \quad (7)$$

where ξ denotes the local cloud cover fraction, %.

The downwelling atmospheric longwave radiation of a clear sky can be expressed by:

$$Q_{atm,clear} = 2\pi \int_0^{0.5\pi} \sin\theta \cos\theta d\theta \int_0^\infty I_{BB}\left(\left(T_{air} + 273.15\right), \lambda\right) \varepsilon_{roof}(\lambda, \theta) \varepsilon_{atm}(\lambda, \theta) d\lambda \quad (8)$$

where $\varepsilon_{atm}(\lambda, \theta)$ denotes the atmospheric emissivity, and it can be calculated by:

$$\varepsilon_{atm}(\lambda, \theta) = 1 - [1 - \varepsilon_{atm}(\lambda, 0)]^{1/\cos\theta} = 1 - [\tau(\lambda)]^{1/\cos\theta} \quad (9)$$

where $\varepsilon_{atm}(\lambda, 0)$ is the atmospheric emissivity of deep space; $\tau(\lambda)$ is the atmospheric transmissivity at the zenith direction; and $\tau(\lambda)$ is calculated with the MODTRAN model [26].

For heat transfer in the cloud, the cloud is usually simplified as a black body. Thus, the downwelling radiation from the cloud can be expressed by [27]:

$$Q_{atm,cloudy} = \vartheta(T_{cloud} + 273.15)^4 \quad (10)$$

where ϑ is the Stefan-Boltzmann constant, $W/(m^2 \cdot K^4)$. The cloud base temperature T_{cloud} can be evaluated from the cloud cover fraction:

$$T_{cloud} = \Delta T_{ref} \ln(\xi) + T_{air} \quad (11)$$

where ΔT_{ref} means the reference temperature difference between T_{cloud} and T_{air} . The cloud emissivity is 100% in the atmospheric window of 8–13 μm because the cloud mainly consists of water crystals. The ΔT_{ref} is assumed to be 10 °C [27].

If the sky is fully covered by the cloud ($\xi = 1$), the cloud temperature is near the earth's surface temperature and acts as a black body ($T_{cloud} \approx T_{air}$). If the sky is partially covered

by clouds ($\zeta < 1$), the cloud tends to be higher and colder, and the cloud cover fraction is exponentially proportional to the cloud base temperature [27]:

$$\zeta = \exp\left(-\frac{T_{air}-T_{cloud}}{\Delta T_{ref}}\right) \quad (12)$$

However, for some small cities, it is very difficult to obtain the cloud cover fraction from local weather observations. Given this situation, the cloud cover fraction can be calculated with the following equation:

$$\zeta = 1 - \frac{G_{solar}}{G_{solar,clear-sky}} \quad (13)$$

where G_{solar} is the actual solar radiation from the observations, and $G_{solar,clear-sky}$ is the theoretical solar radiation under clear weather conditions, and it can be calculated through the solar prediction model developed by Yang et al. [28].

The solar radiation absorbed by the rooftop surface can be calculated by:

$$Q_{solar} = \int_0^{\infty} I_{AM1.5}(\lambda) \varepsilon_{cc}(\lambda, \theta_{solar}) d\lambda \quad (14)$$

where $I_{AM1.5}$ refers to the standard terrestrial solar spectral irradiance spectra.

The convective heat transferred on the top roof surface can be calculated by:

$$Q_{convection} = h_{cov} A_{roof} (T_{air} - T_{roof}) \quad (15)$$

Here, h_{cov} is the convective heat transfer coefficient between the roof and ambient environment, $W/(m^2 \cdot K)$, which is a function of wind velocity (v_{air}) and can be obtained by [29]:

$$h_{cov} = 8.55 \pm 0.86 + 2.56 \pm 0.32 v_{wind} \quad (16)$$

The indoor ceiling exchanges heat with walls and windows, for which the temperature can be calculated by:

$$Q_{ceiling} = Q_{id-roof} + Q_{wall,S-roof} + Q_{wall,N-roof} + Q_{wall,W-roof} + Q_{wall,E-roof} + Q_{wd,S-roof} + Q_{wd,N-roof} + Q_{wd,W-roof} + Q_{wd,E-roof} \quad (17)$$

The $Q_{id-roof}$ is the heat exchanged between the ceiling and the indoor environment, which is introduced in Equation (25).

The $Q_{wall,S-roof}$ is the heat exchange rate between the indoor ceiling and the south wall, which can be calculated by:

$$Q_{wall,S-roof} = \theta_1 (Q_{rad,wall,S} - Q_{rad,roof}) \quad (18)$$

where $Q_{rad,wall,S}$ is the radiated-out heat of the south wall, which can be calculated by Equation (5). The ε_{cc} in Equation (5) should be replaced by the ε_{wall} of the wall. $Q_{rad,roof}$ is the radiated-out heat of the ceiling, which can also be calculated with Equation (5). The ε_{cc} in Equation (5) should be replaced with the $\varepsilon_{ceiling}$ of the ceiling.

The $Q_{wall,S-wd}$ is the heat exchange rate between the indoor ceiling and the south window, which can be calculated by:

$$Q_{wall,S-wd} = \theta_2 (Q_{rad,wd,S} - Q_{rad,roof}) \quad (19)$$

where θ_1 and θ_2 are the view factors between the ceiling and walls and between the ceiling and windows, respectively. $Q_{rad,wd,S}$ is the radiated-out heat of the window, which can also be calculated with Equation (5). The ε_{cc} in Equation (5) should be replaced by the ε_{wd} of the window.

The calculation equations of heat exchanged between the ceiling and other walls and windows are similar to the above equations. To make the text more compact, they will not be expressed again.

3.2. Window Models

Low-E windows include two layers, and their heat transfer mechanism is different. The outdoor-side Low-E window exchanges heat with the outdoor environment and the indoor-side glass. Thus, the control equation of the outdoor-side glass can be expressed by:

$$-\rho_{wd1}c_{wd1}V_{wd1}\frac{dT_{wd1}}{dt} = A_{wd}Q_{wd1-wd2} + A_{wd}Q_{net,wd1} \quad (20)$$

The heat exchanged between the inner and outer glass can be calculated by:

$$Q_{wd1-wd2} = Q_{rad,wd1} - Q_{rad,wd2} + h_{cov,wd}(T_{wd2} - T_{wd1}) + \frac{k_{cov,airc}(T_{wd2} - T_{wd1})}{\delta_{airc}} \quad (21)$$

where $Q_{net,wd1}$ is the net cooling power of the window; $Q_{rad,wd1}$ is the radiated-out heat of the outer window. $Q_{rad,wd2}$ is the radiated-out heat of the inner window. δ_{airc} is the spacing between the inner and outer window, m. When the gap between these two layers of glass is a vacuum, the $h_{cov,wd}$ and $k_{cov,airc}$ are both zero.

The outgoing radiative cooling power of the indoor-side glass and the outdoor-side glass can be calculated by:

$$Q_{rad,wd1} = 2\pi \int_0^{0.5\pi} \sin\theta \cos\theta d\theta \int_0^\infty I_{BB}((T_{wd1} + 273.15), \lambda) \varepsilon_{wd1}(\lambda, \theta) d\lambda \quad (22)$$

$$Q_{rad,wd2} = 2\pi \int_0^{0.5\pi} \sin\theta \cos\theta d\theta \int_0^\infty I_{BB}((T_{wd2} + 273.15), \lambda) \varepsilon_{wd2}(\lambda, \theta) d\lambda \quad (23)$$

The indoor-side window temperature can be calculated by:

$$-\rho_{wd2}c_{wd2}V_{wd2}\frac{dT_{wd2}}{dt} = A_{wd}Q_{wd2-wd1} + A_{wd}Q_{indoor,wd2} \quad (24)$$

where $Q_{wd2-wd1}$ equals $Q_{wd1-wd2}$; $Q_{indoor,wd2}$ is the exchange heat between the inner window and the indoor environment, which is introduced in Equation (25).

3.3. Wall Models

The heat transfer processes of the walls are similar to the building roof. Thus, the calculation equations of the four surrounding walls are similar to the equations of the roof. In order to make the text more compact, the calculation equations are not demonstrated. It should be noted that the north wall is not affected by solar radiation.

3.4. Indoor Model

The indoor air mainly exchanges heat with the surroundings by convective heat transfer. Due to the high transparency of air, the radiative heat transfer is ignored and thus can be calculated by:

$$\begin{aligned} -\rho_{indoor}c_{indoor}V_{indoor}\frac{dT_{id}}{dt} = & A_{ceiling}h_{id}(T_{roof} - T_{id}) + A_{wall}h_{id}(T_{wall,S} - T_{id}) \\ & + A_{wall}h_{id}(T_{wall,N} - T_{id}) + A_{wall}h_{id}(T_{wall,W} - T_{id}) + A_{wall}h_{id}(T_{wall,E} - T_{id}) \\ & + A_{wd}h_{id}(T_{wd,S} - T_{id}) + A_{wd}h_{id}(T_{wd,N} - T_{id}) + A_{wd}h_{id}(T_{wd,W} - T_{id}) \\ & + A_{wd}h_{id}(T_{wd,E} - T_{id}) + A_{window}Q_{id,solar} \end{aligned} \quad (25)$$

where $Q_{id,solar}$ is the indoor incoming solar radiation through the windows.

The cooling load relates to the indoor air temperature variations, which can be calculated by:

$$Q_{load} = -\rho_{indoor}c_{indoor}V_{indoor}\frac{dT_{id}}{dt} \quad (26)$$

4. Model Validations

To verify the developed building model, the roof and window temperatures calculated by the developed model are compared with those of the experiments (see Figure 2). It should be noted that the roof and window temperatures are validated with two separate experiments, and the basic model settings are the same as those in the correspondingly cited references. In detail, firstly, the experimental data of cooling roofs are cited from ref. [30]. In this experiment, which was carried out in Hong Kong, a size-reduced box was used to mimic the room. Then, the Low-E window temperature is validated with an experiment in ref. [31], which was carried out in Hefei, China. The temperature profiles for the roof and windows show similar trends. In the morning, the temperatures increase as the solar radiation increases, and then the temperatures drop gradually in the afternoon. As shown, the simulated results agree well with the experimental results. Obviously, the relative errors for roof and window temperatures are both smaller than 5%. Thus, the developed model can provide a reliable tool for further discussion.

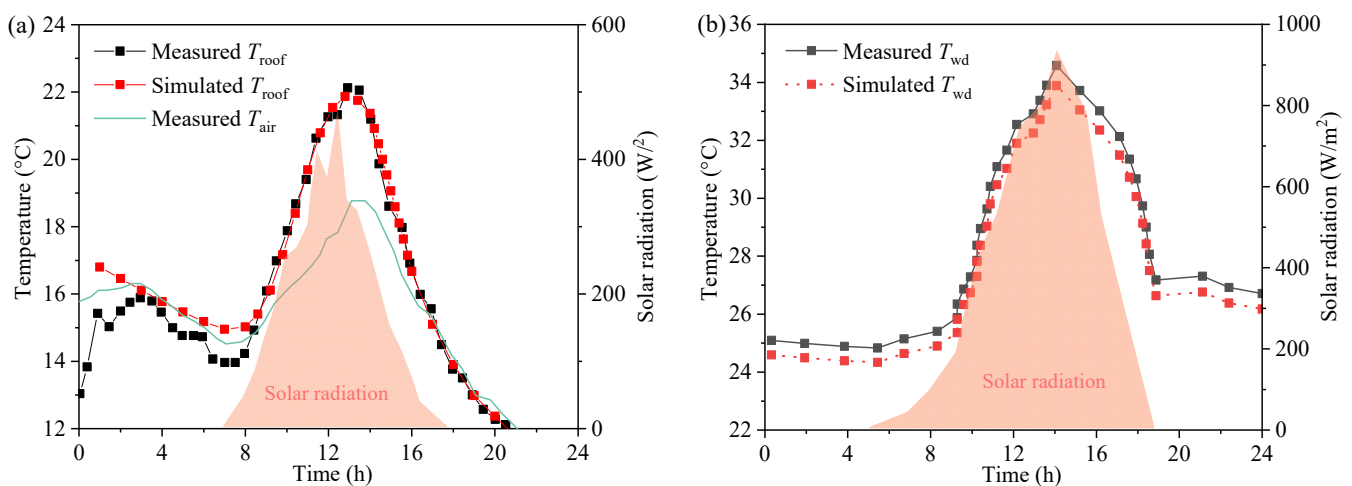


Figure 2. Comparison of simulation and experimental results. (a) Roof temperatures; (b) window temperatures.

5. Calculation Description

5.1. Spectral Properties of the Roof, Walls, and Windows

The radiative heat transfer on the roof, walls, and windows mainly depends on their spectral properties. Due to their different purposes, the roof and walls are expected to show larger solar reflectance in wavelengths of 0–2.5 μm and to show larger thermal emittance in the far-infrared thermal region. Compared with the spectral properties of roofs and walls, Low-E windows should allow visible light into the indoor environment to guarantee basic illumination. Thus, in the visible region, a lower reflectance is needed. Figure 3 shows the spectral properties of the roof (walls) and windows. Compared with practical cooling coatings, using an ideal spectrum can achieve the best cooling performance. To make this study more representative of the practical application of this cooling building technology worldwide, the ideal spectra are used for the following analysis.

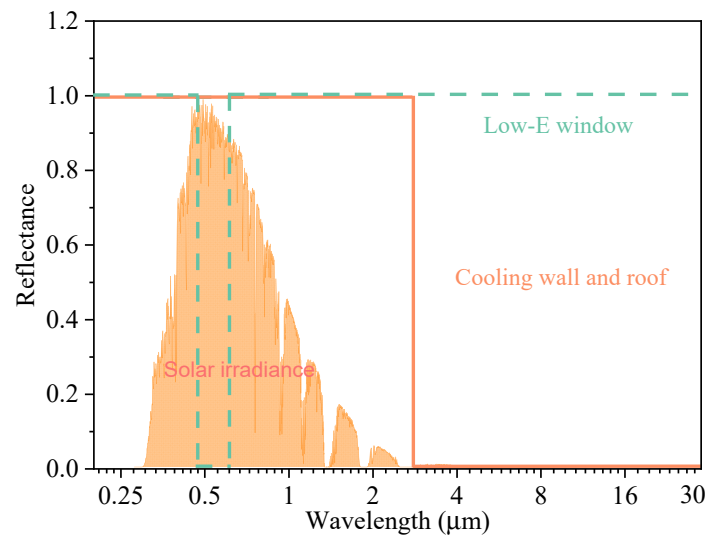


Figure 3. Spectral properties of the roof and windows.

5.2. Atmospheric Transmittance

The absorbed downwelling atmospheric radiation by the radiative cooling surface depends not only on the spectral properties of the coatings but also the atmospheric emissivity, which can be approximated by the water vapour column (WVC). Undoubtedly, the spectrally dependent atmospheric transmissivity $\tau(\lambda)$ relates to multiple environmental variables, including CO₂ concentrations, atmosphere pressure, WVC, cloud thickness, etc. [32]. Among all the experimental factors, the WVC levels can significantly affect the calculation of $\tau(\lambda)$, and it is therefore considered in detail [21]. The cloud variations may also affect the $\tau(\lambda)$. However, it is not considered herein since its high uncertainty is related to many hard-to-predict factors such as the cloud shape, thickness, temperature, altitude, and angular position [33].

Figure 4 shows the $\tau(\lambda)$ from 2 to 16 μm with different WVCs. As shown, the WVCs mainly influence the $\tau(\lambda)$ amid the atmospheric window (8–13 μm). The average $\tau(\lambda)$ amid atmospheric windows are 0.77, 0.70, 0.61, and 0.56 for 1000, 2000, 3000, and 4000 atm-cm, respectively. It should be noted that higher WVCs can lead to smaller atmospheric transmissivity, indicating that more downward atmospheric thermal radiation is radiated to the roofs. Thus, the roof is expected to operate under a clear sky with low WVCs.

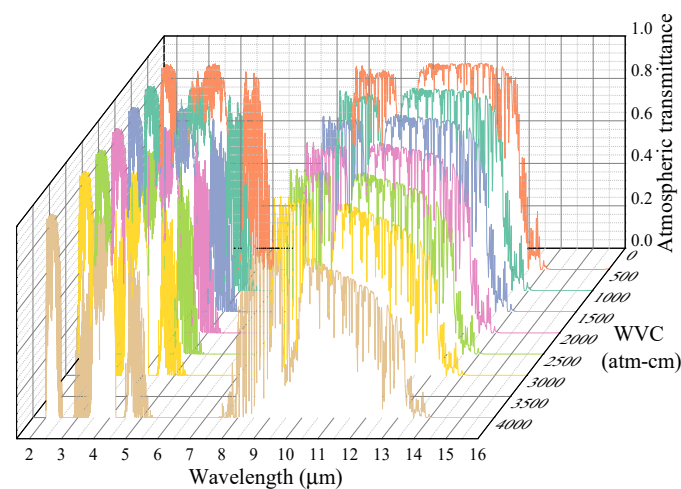


Figure 4. Atmospheric transmittances with different WVCs.

5.3. Weather Data for Hong Kong

Due to the hot and humid ambient conditions in Hong Kong, which is located in a tropical region, the cooling demands are tremendous. Analysing the performance of buildings in this region can be representative. Therefore, Hong Kong is selected as the target research region. Figure 5 shows the hourly weather data for Hong Kong, including the solar radiation (G_{solar}), ambient temperature (T_{air}), relative humidity (RH), and water vapour column (WVC), derived from the Hong Kong observatory. As shown, Hong Kong features high G_{solar} , T_{air} , RH, and WVC in the summer months, indicating the larger requirement for indoor cooling power.

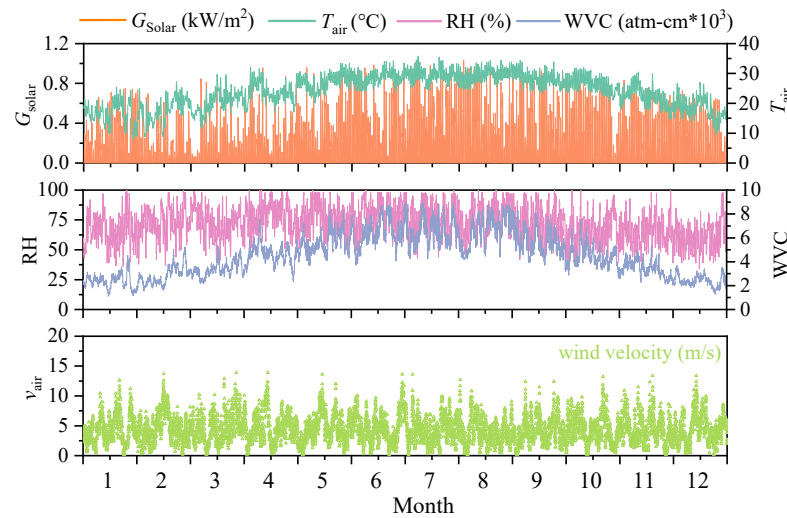


Figure 5. Weather data for Hong Kong.

6. Results and Analyses

6.1. Calculation Description

In this section, the cooling responses of the buildings in Hong Kong are first analysed. The hourly calculated results are presented and discussed. It should be noted that the local weather conditions can significantly influence the cooling demands of buildings. To provide general suggestions on the cooling potential of this sky-cooling technology, the national-based map of energy-saving potential across China is given in this section. The cooling division map of the cooling demands in China during the summer months is depicted. The corresponding equation is shown in Equation (27).

$$Q_{\text{load, summer}} = \frac{\int_0^{t_{\text{summer}}} Q_{\text{load}}(t) dt}{\sum t_{\text{summer}}} \quad (27)$$

where t_{summer} denotes the total summer hours, h.

It should be noted that in some remote areas, it is difficult to obtain enough weather data from weather observations. Thus, in order to obtain the local weather data, an inverse distance weighting spatial interpolation method is used to calculate the weather data. Equation (27) lists the corresponding equation for this method.

$$\hat{Z} = \frac{\sum_{i=1}^N w(d_i) Z_i}{\sum_{i=1}^N w(d_i)} \quad (28)$$

where N is the number of stations; d_i is the geographic distance between station i and the target location, km; Z_i is the variable at station i ; and $w(d_i)$ is the weighting function that inversely depends on the distance d as follows:

$$w(d) = \frac{1}{d^p}, p = 1 \quad (29)$$

$$d = 2r \arcsin \left(\sqrt{\sin^2 \left(\frac{\varphi_2 - \varphi_1}{2} \right) + \cos(\varphi_2) \cos(\varphi_1) \sin^2 \left(\frac{\omega_2 - \omega_1}{2} \right)} \right) \quad (30)$$

Here, r is the radius of the earth sphere, km; φ_1 , φ_2 are the latitudes of location 1 and location 2, rad. ω_1 and ω_2 are the longitudes of location 1 and location 2, rad.

In total, 255 cities across China are selected as research targets. Their corresponding cooling demands are calculated, considering the locally typical year meteorological data derived from the EnergyPlus weather database. The performance of cooling roofs and Low-E windows is closely linked to prevailing weather conditions. The present study considers several key weather parameters, including T_{air} , G_{solar} , v_{air} , and WVC, as shown in Figure 6a–d, presenting the annual average weather data.

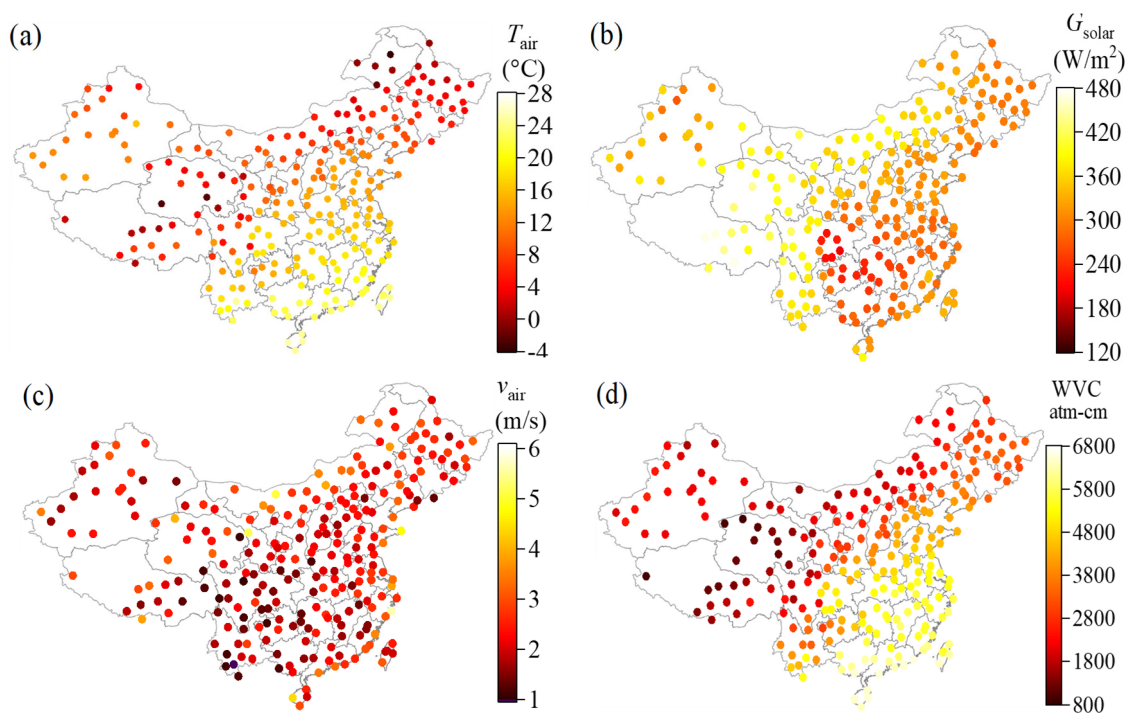


Figure 6. Annual average cooling resources. (a) T_{air} ; (b) G_{solar} ; (c) v_{air} ; and (d) WVC.

6.2. Temperature Responses

The roof, wall, window, and indoor temperatures show daily dynamic profiles. Figure 7a,b demonstrate 5-day roof, wall, window, and indoor temperatures for standard and cooling buildings, respectively. Figure 8 shows the cooling loads in summer months for standard buildings and cooling buildings.

For conventional buildings, the roof temperature shows maximum amplitudes, as shown in Figure 7. The roof temperature maximum peaks under sunlight and drops to the minimum at night. For the temperature responses, the south wall shows the highest temperature, and the north wall shows the lowest temperature. The east and west walls exhibit distinctly different temperature responses. The east wall demonstrates a higher temperature than the west wall, while the west wall shows a higher temperature in the afternoon. The indoor temperature is relatively higher than the south wall temperature but lower than the top roof temperature. The high indoor temperature is attributed to the large heat flux transferred from the outdoors into the indoors. The indoor cooling demand can reach 75 W/m^2 in September. Compared with standard buildings, the cooling building shows better cooling performances due to the coated cooling materials on the roof, walls, and windows. As shown in Figure 8, the indoor temperature can be sub-ambient. The cooling demands for a cooling building are reduced from 75.0 W/m^2 to 30.0 W/m^2 , showing a 60% energy savings.

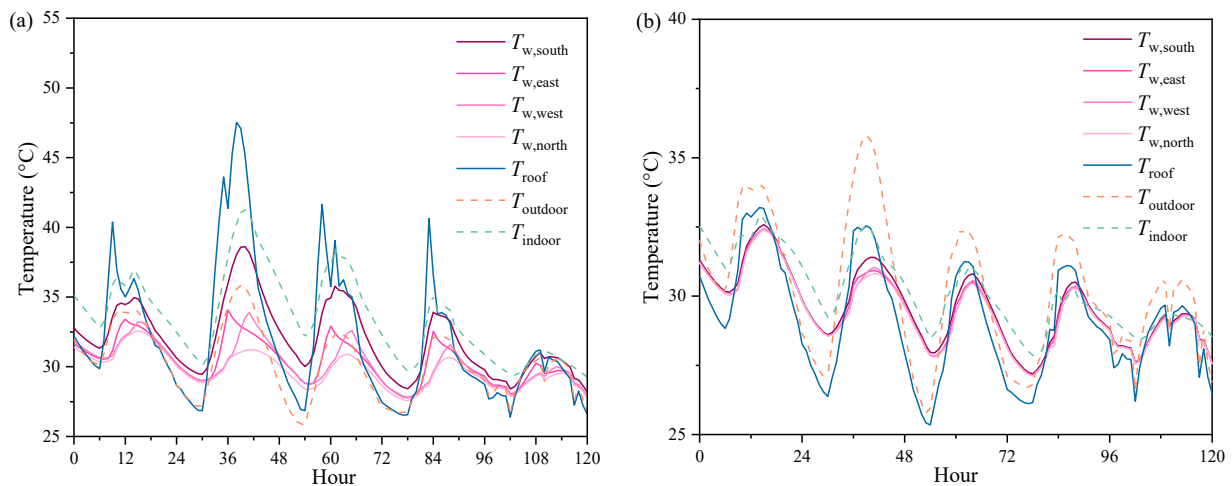


Figure 7. Temperature variations on typical summer days. (a) Standard building without cooling coating and Low-E windows. (b) Cooling building with cooling coating and Low-E windows.

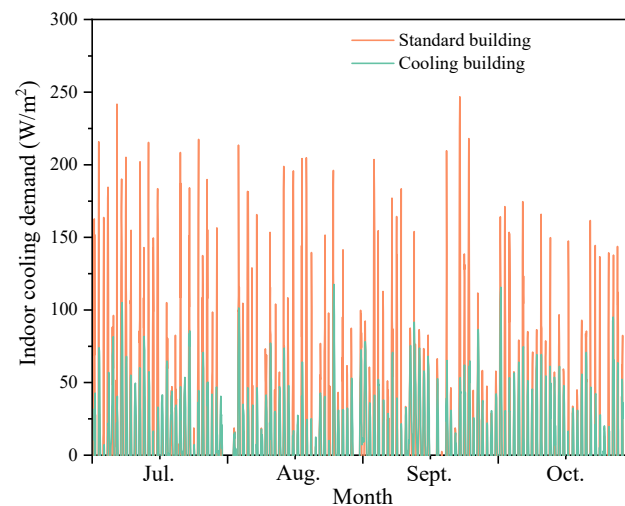


Figure 8. Cooling loads in summer months for a standard building and a cooling building.

6.3. Cooling Division Map in China

Figure 9a shows the map of cooling demands for standard buildings across China. As shown, the southern cities need more cooling demands due to the hot weather conditions. By contrast, the northern cities show the lowest indoor cooling powers because of the cold and dry weather conditions. The nationwide cooling demand of standard buildings across China reaches up to 95.7 W/m².

In comparison to standard buildings, the cooling requirements of cooling buildings across China show lower levels, ascribed to the cooling coating on roofs and walls and Low-E windows. In southern cities, the maximum cooling demand is about 65.1 W/m², as shown in Figure 9b. The cooling demands in northern cities drop to 30.7 W/m². The nationwide summer average cooling demand is 52.7 W/m².

Compared with that for standard buildings, the cooling demand for cooling buildings is reduced by 35.7% on a nationwide level. Specifically, in southern regions, the energy-saving potentials are more obvious due to the original huge indoor cooling demands. As shown in Figure 9c, in South China, 60.5% of indoor cooling demand can be saved. In North China, the energy-saving potential is relatively smaller, with an indoor cooling reduction of 30.7%. Overall, using the proposed cooling building with Low-E windows can effectively reduce indoor cooling requirements.

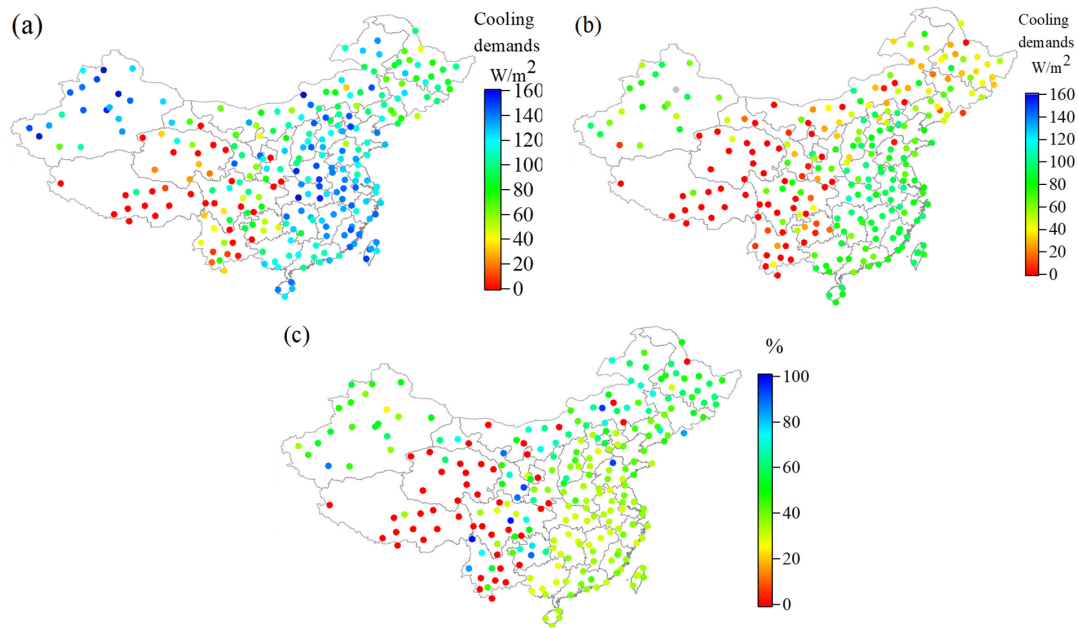


Figure 9. Annual average cooling resources. (a) Cooling demands for a standard building; (b) cooling demands for a cooling building; (c) energy-saving potential between standard and cooling buildings.

6.4. Cooling Performance of a Cooling Roof

The lower indoor cooling demands are ascribed to the better cooling performances of cooling buildings, which can passively radiate heat from the building to the environment. Compared with walls, the roof has better cooling potential due to the larger sky view factor. Specifically, the roof can radiate heat to the entire sky, but the walls have only half the sky view factor. Thus, the temperature difference between the ambient temperature and roof temperature for standard and cooling buildings is shown in Figure 10.

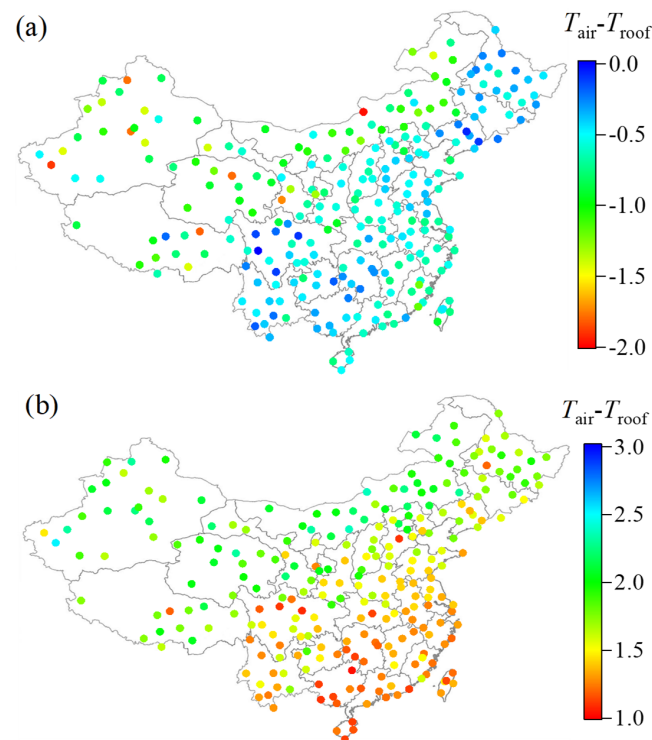


Figure 10. Temperature drops on the roof for standard buildings and cooling buildings. (a) Standard buildings; (b) cooling buildings.

For the standard buildings, as shown in Figure 10a, the roof temperature is higher than the ambient air temperature, due to the high solar absorption. After coating the cooling materials and using a Low-E window, the roof temperature can be lower than the ambient temperature, as shown in Figure 10b. Noticeably, the cooling performance of the roof is significantly related to the weather conditions. The hot and humid weather conditions are harmful to the cooling performance of the cooling roof. Thus, in southern regions, the temperature drops of cooling roofs are relatively lower than those in northern regions. Overall, the nationwide temperature drop across China is $1.6\text{ }^{\circ}\text{C}$, which shows promising cooling potential.

6.5. Cooling Performance of Low-E Windows

In order to guarantee basic indoor lighting, Low-E windows should allow visible light into the indoor environment. As a result, the majority of indoor cooling requirements are attributed to visible solar light. In this section, the energy-saving potential of Low-E windows compared to standard windows across China is presented. Due to the direction, the performance of south windows is more important and is analysed in the following context.

In comparison to standard windows, Low-E windows allow only light in the wavelength of 400–700 nm into the indoor environment. In addition, in the infrared thermal region, Low-E windows have a larger thermal emittance, which can radiate more heat to the environment. As shown in Figure 11a, the summer average temperature drop of standard windows across China is shown, and the nationwide temperature drop across China is $-1.8\text{ }^{\circ}\text{C}$. For Low-E windows, the Low-E temperature can be sub-ambient, with a nationwide average temperature drop of $1.7\text{ }^{\circ}\text{C}$, as shown in Figure 11b. Thus, using Low-E windows across China can definitively save energy on indoor cooling purposes.

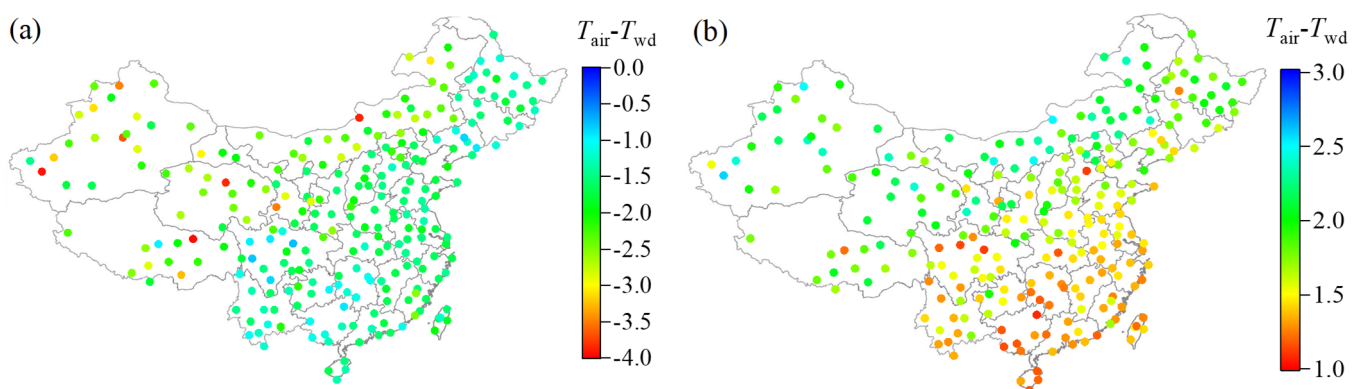


Figure 11. Temperature drops for the south windows of standard buildings and cooling buildings. (a) Standard buildings; (b) cooling buildings.

7. Discussion

Undeniably, the category of building construction, the construction materials, and even the building orientations can affect indoor cooling demands, which deserves a detailed analysis. In different areas, building materials vary geographically, which poses challenges in comparing the cooling demands fairly. Usually, low-conductivity materials are applied to fabricate walls and roofs because low-conductivity materials can limit the heat transferred from the outdoor environment and indoor environment. Please note that a building's envelope properties are influenced by the climate and are designed according to the building energy code specified in ANSI/ASHRAE/IES Standard 90.1—2019 [34]. The building type chosen in this study is 1 of the 16 building types identified by the Building Energy Codes Program. These building types are representative of approximately 70% of commercial buildings. Therefore, the selected building type serves as a realistic representation of commercial buildings. However, the relevant results in this study are

only available for commercial buildings due to the specific construction settings. For other kinds of building types, the corresponding cooling performances can be regarded as a future direction.

8. Conclusions

This study develops a building with a cooling roof, walls, and Low-E windows. The developed model is verified by the experimental data related to the roof, walls, windows and indoor temperatures. A comparison of the cooling demands is made between standard buildings and cooling buildings, and the energy-saving potential of cooling buildings is analysed. The cooling performances of the cooling roof and Low-E windows across China are elaborated on in detail. The main conclusions are summarized as follows:

- (1) A cooling coating and Low-E window-assisted building model is developed using numerical methods. The developed numerical model is verified by comparing the temperature responses with the experimental data, demonstrating promising prediction accuracy for further discussion;
- (2) Compared with standard buildings, cooling buildings show a better cooling performance due to the coated cooling materials on the roof, walls, and windows. In a case considering Hong Kong weather data, the indoor temperature could reach sub-ambient levels. The cooling demands for cooling buildings are reduced from 75 W/m² to 30 W/m², resulting in a 60% energy savings;
- (3) The nationwide cooling demand of standard buildings across China reaches up to 95.7 W/m². In contrast, cooling buildings equipped with cooling coatings on roofs and walls as well as Low-E windows show lower cooling requirements across the country. The average nationwide summer cooling demand is 52.7 W/m²;
- (4) Hot and humid weather conditions have a detrimental effect on the cooling performance of a cooling roof. Thus, the temperature decreases for cooling roofs in southern regions are relatively lower than those in northern regions. Overall, the nationwide temperature drop across China is 1.6 °C, which shows promising cooling potential;
- (5) Low-E windows can be used to achieve sub-ambient temperatures, leading to an average nationwide temperature reduction of 1.7 °C. Thus, using Low-E windows across China has the potential to significantly conserve energy for indoor cooling purposes.

Author Contributions: Writing—original draft preparation, L.-R.J.; Visualization, Editing, Q.-Y.L.; Investigation, Resources, J.Y.; Supervision, Conceptualization, Writing—review and editing, Funding acquisition, and Project administration, J.H.; Supervision, C.-C.L.; and Editing, J.-H.C. All authors have read and agreed to the published version of the manuscript.

Funding: This work was financially supported by the Research Grants Council of the Hong Kong Special Administrative Region, China (UGC/FDS16/P01/20).

Data Availability Statement: Data are contained within the article.

Conflicts of Interest: Author Jie Yang was employed by the company Joinhuger Group Co. Ltd., China. The remaining authors declare that the research was conducted in the absence of any commercial or financial relationships that could be construed as a potential conflict of interest.

References

1. Elder, T.; Strong, J. The infrared transmission of atmospheric windows. *J. Frankl. Inst.* **1958**, *255*, 189–208. [[CrossRef](#)]
2. Ziming, C.; Fuqiang, W.; Dayang, G.; Huaxu, L.; Yong, S. Low-cost radiative cooling blade coating with ultrahigh visible light transmittance and emission within an “atmospheric window”. *Sol. Energy Mater. Sol. Cells* **2020**, *213*, 110563. [[CrossRef](#)]
3. Yin, X.; Yang, R.; Tan, G.; Fan, S. Terrestrial radiative cooling: Using the cold universe as a renewable and sustainable energy source. *Science* **2020**, *370*, 786–791. [[CrossRef](#)]
4. Chen, H.; Li, Z.; Sun, B. Performance evaluation and parametric analysis of an integrated diurnal and nocturnal cooling system driven by photovoltaic-thermal collectors with switchable film insulation. *Energy Convers. Manag.* **2022**, *254*, 115197. [[CrossRef](#)]

5. Bagiorgas, H.S.; Mihalakakou, G. Experimental and theoretical investigation of a nocturnal radiator for space cooling. *Renew. Energy* **2008**, *33*, 1220–1227. [[CrossRef](#)]
6. Zhai, Y.; Ma, Y.; David, S.N.; Zhao, D.; Lou, R.; Tan, G.; Yang, R.; Yin, X. Scalable-manufactured randomized glass-polymer hybrid metamaterial for daytime radiative cooling. *Science* **2017**, *355*, 1062–1066. [[CrossRef](#)]
7. Atiganyanun, S.; Plumley, J.B.; Han, S.J.; Hsu, K.; Cytrynbaum, J.; Peng, T.L.; Han, S.M.; Han, A.S.E. Effective radiative cooling by paint-format microsphere-based photonic random media. *ACS Photonics* **2018**, *5*, 1181–1187. [[CrossRef](#)]
8. Raman, A.P.; Anoma, M.A.; Zhu, L.; Rephaeli, E.; Fan, S. Passive radiative cooling below ambient air temperature under direct sunlight. *Nature* **2014**, *515*, 540–544. [[CrossRef](#)]
9. Mandal, J.; Fu, Y.; Overvig, A.C.; Jia, M.; Sun, K.; Shi, N.N.; Zhou, H.; Xiao, X.; Yu, N.; Yang, Y. Hierarchically porous polymer coatings for highly efficient passive daytime radiative cooling. *Science* **2018**, *362*, 315–331. [[CrossRef](#)]
10. Li, D.; Liu, X.; Li, W.; Lin, Z.; Zhu, B.; Li, Z.; Li, J.; Li, B.; Fan, S.; Xie, J.; et al. Scalable and hierarchically designed polymer film as a selective thermal emitter for high-performance all-day radiative cooling. *Nat. Nanotechnol.* **2021**, *16*, 153–158. [[CrossRef](#)]
11. Zinzi, M.; Agnoli, S. Cool and green roofs. An energy and comfort comparison between passive cooling and mitigation urban heat island techniques for residential buildings in the Mediterranean region. *Energy Build.* **2012**, *55*, 66–76. [[CrossRef](#)]
12. Yew, M.C.; Yew, M.K.; Saw, L.H.; Ng, T.C.; Chen, K.P.; Rajkumar, D.; Beh, J.H. Experimental analysis on the active and passive cool roof systems for industrial buildings in Malaysia. *J. Build. Eng.* **2018**, *19*, 134–141. [[CrossRef](#)]
13. Tian, D.; Zhang, J.; Gao, Z. The advancement of research in cool roof: Super cool roof, temperature-adaptive roof and crucial issues of application in cities. *Energy Build.* **2023**, *291*, 113131. [[CrossRef](#)]
14. Zhu, L.; Raman, A.; Wang, K.X.; Anoma, M.A.; Fan, S. Radiative cooling of solar cells. *Optica* **2014**, *1*, 32–38. [[CrossRef](#)]
15. Ahmadi, F.; Wilkinson, S.; Rezazadeh, H.; Keawsawasvong, S.; Najafi, Q.; Masoumi, A. Energy efficient glazing: A comparison of microalgae photobioreactor and Iranian Orosi window designs. *Build. Environ.* **2023**, *233*, 109942. [[CrossRef](#)]
16. Cots, A.; Dicorato, S.; Giovannini, L.; Favoino, F.; Manca, M. Energy Efficient Smart Plasmochromic Windows: Properties, Manufacturing and Integration in Insulating Glazing. *Nano Energy* **2021**, *84*, 105894. [[CrossRef](#)]
17. Kaushik, N.; Saravanakumar, P.; Dhanasekhar, S.; Saminathan, R.; Rinawa, M.L.; Subbiah, R.; Sharma, R.; Manoj Kumar, P. Thermal analysis of a double-glazing window using a Nano-Disbanded Phase Changing Material (NDPCM). *Mater. Today Proc.* **2022**, *62*, 1702–1707. [[CrossRef](#)]
18. Ghosh, A. Investigation of vacuum-integrated switchable polymer dispersed liquid crystal glazing for smart window application for less energy-hungry building. *Energy* **2023**, *265*, 126396. [[CrossRef](#)]
19. Zhang, C.; Ji, J.; Wang, C.; Ke, W.; Xie, H.; Yu, B. Experimental and numerical studies on the thermal and electrical performance of a CdTe ventilated window integrated with vacuum glazing. *Energy* **2022**, *244*, 123128. [[CrossRef](#)]
20. Huang, Y.; El Mankibi, M.; Cantin, R.; Coillot, M. Application of fluids and promising materials as advanced inter-pane media in multi-glazing windows for thermal and energy performance improvement: A review. *Energy Build.* **2021**, *253*, 111458. [[CrossRef](#)]
21. Zhu, Y.; Qian, H.; Yang, R.; Zhao, D. Radiative sky cooling potential maps of China based on atmospheric spectral emissivity. *Sol. Energy* **2021**, *218*, 195–210. [[CrossRef](#)]
22. Chen, J.; Lu, L. Comprehensive evaluation of thermal and energy performance of radiative roof cooling in buildings. *J. Build. Eng.* **2021**, *33*, 101631. [[CrossRef](#)]
23. Urbikain, M.K. Energy efficient solutions for retrofitting a residential multi-storey building with vacuum insulation panels and low-E windows in two European climates. *J. Clean. Prod.* **2020**, *269*, 121459. [[CrossRef](#)]
24. Yunos, L.; Jane, M.L.; Murphy, P.J.; Zuber, K. Frequency selective surface on low emissivity windows as a means of improving telecommunication signal transmission: A review. *J. Build. Eng.* **2023**, *70*, 106416. [[CrossRef](#)]
25. Chen, J.; Gong, Q.; Lu, L. Evaluation of passive envelope systems with radiative sky cooling and thermally insulated glazing materials for cooling. *J. Clean. Prod.* **2023**, *398*, 136607. [[CrossRef](#)]
26. Berk, A.; Conforti, P.; Hawes, F. An Accelerated Line-By-Line Option for MODTRAN Combining On-The-Fly Generation of Line Center Absorption within 0.1 cm⁻¹ Bins and Pre-computed Line Tails, Algorithms and Technologies for Multispectral, Hyperspectral, and Ultraspectral Imagery XXI. *Int. Soc. Opt. Photonics* **2015**, *9472*, 405–415.
27. Aili, A.; Yin, X.; Yang, R. Global Radiative Sky Cooling Potential Adjusted for Population Density and Cooling Demand. *Atmosphere* **2021**, *12*, 1379. [[CrossRef](#)]
28. Yang, K.; Koike, T.; Ye, B. Improving estimation of hourly, daily, and monthly solar radiation by importing global data sets. *Agric. For. Meteorol.* **2006**, *137*, 43–55. [[CrossRef](#)]
29. Bliss, J.R. Atmospheric radiation near the surface of the ground: A summary for engineers. *Sol. Energy* **1961**, *5*, 103–120. [[CrossRef](#)]
30. Chen, J.; Lu, L.; Gong, Q.; Wang, B.; Jin, S.; Wang, M. Development of a new spectral selectivity-based passive radiative roof cooling model and its application in hot and humid region. *J. Clean. Prod.* **2021**, *307*, 127170. [[CrossRef](#)]
31. Uddin, M.M.; Wang, C.; Zhang, C.; Ji, J. Investigating the energy-saving performance of a CdTe-based semi-transparent photovoltaic combined hybrid vacuum glazing window system. *Energy* **2022**, *253*, 124019. [[CrossRef](#)]
32. Zhao, D.; Aili, A.; Zhai, Y.; Lu, J.; Kidd, D.; Tan, G.; Yin, X.; Yang, R. Subambient Cooling of Water: Toward Real-World Applications of Daytime Radiative Cooling. *Joule* **2019**, *3*, 111–123. [[CrossRef](#)]

33. Aili, A.; Zhao, D.; Lu, J.; Zhai, Y.; Yin, X.; Tan, G.; Yang, R. A kW-scale, 24-hour continuously operational, radiative sky cooling system: Experimental demonstration and predictive modelling. *Energy Convers. Manag.* **2019**, *186*, 586–596. [[CrossRef](#)]
34. *ANSI/ASHRAE/IES Standard 90.1-2019*; Energy Efficiency Standard for Buildings Except Low-Rise Residential Buildings. ASHRAE: Peachtree Corners, GA, USA, 2019. Available online: <https://www.ashrae.org/news/hvacindustry/2019-update-of-standard-90-1> (accessed on 1 November 2023).

Disclaimer/Publisher’s Note: The statements, opinions and data contained in all publications are solely those of the individual author(s) and contributor(s) and not of MDPI and/or the editor(s). MDPI and/or the editor(s) disclaim responsibility for any injury to people or property resulting from any ideas, methods, instructions or products referred to in the content.